JGR Solid Earth

Key Points:
- An updated archaeomagnetic regional model for Europe for the last 4,000 years
- A better knowledge of the spatial and temporal past evolution of the European geomagnetic field
- The regional model can be used as a tool for archaeomagnetic dating in Europe

Supporting Information:
- Supporting Information S1
- Table S1
- Movie S1

Correspondence to:

F. J. Pavón-Carrasco,
fjpavon@ucm.es

SCHA.DIF.4k: 4,000 Years of Paleomagnetic Reconstruction for Europe and Its Application for Dating

F. Javier Pavón-Carrasco[1] , Saioa A. Campuzano[2] , Mercedes Rivero-Montero[1,2] , Alberto Molina-Cardín[1,2] , Miriam Gómez-Paccard[2] , and M. Luisa Osete[1,2]

[1]Department of Physics of the Earth and Astrophysics, Facultad de CC. Físicas, Madrid, Spain, [2]Institute of Geosciences IGEO (CSIC – UCM), Madrid, Spain

Abstract Since the publication of the European archaeomagnetic field model SCHA.DIF.3k in 2009, the number of paleomagnetic data derived from archaeological materials such as baked clays and volcanic rocks coming from Europe has increased by about 90% for directions and around 180% for intensities. Taking advantage of this increase, here we provide an updated regional archaeomagnetic model, called SCHA.DIF.4k, for the European continent and adjacent areas and now covering the last four millennia. To model the three geomagnetic elements, declination, inclination, and intensity, we use the regional R-SCHA2D technique in space and temporal basis of cubic splines. A critical selection of the archaeomagnetic and volcanic data available in a spherical cap of 30° centered at 40°N latitude and 10°E longitude has been considered. In addition, in order to better constrain the behavior of the archaeomagnetic field during the last centuries, we include the historical data of the HISTMAG compilation. The new regional model allows us to better define the paleomagnetic field over Europe as well as to generate new paleosecular variation curves for archaeomagnetic dating purposes. Using these curves, the dating precision has been estimated for the last 4 kyr. As expected, results show that it strongly depends on the data uncertainties, the temporal data distribution and the behavior of the geomagnetic field itself. In addition, the use of the full vector geomagnetic field, instead of the directional information exclusively, provides more precise archaeomagnetic dating results.

Plain Language Summary The Earth's magnetic field is generated by complex fluid movements located in the outer core and envelops our planet protecting us against the solar wind. For this reason, the geomagnetic field plays an important role to sustain our life. During the last decades, a worldwide network of observatories and satellites provided an accurate picture of the geomagnetic field changes. Moreover, thanks to the ability of some rocks preserving the ambient geomagnetic field, it is possible to know its past evolution at geological time scales through the so-called paleomagnetic data. For the Holocene, the paleomagnetic information derived from certain archaeological artifacts and lava flows provides snapshots of the past geomagnetic field (or paleofield) and thus, they can be used to reconstruct it at local and global scales. Europe is the continent with a high density of paleomagnetic data for the last four millennia. Taking advantage of this, here we provide a regional reconstruction of the geomagnetic field for this period valid for Europe and adjacent areas. This new model is a useful tool to analyze the paleofield behavior. In addition, it can be used as an improved tool for dating archaeological remains and volcanic rocks from the target region.

1. Introduction

During the last decade, many efforts have been carried out to improve the paleomagnetic database for the Holocene and late Pleistocene epochs. The increase of paleomagnetic data has enabled to have a better knowledge of the spatial and temporal variations of the ancient Earth's magnetic field over the last 100 kyr (Panovska et al., 2019). For the last millennia, the most accurate paleomagnetic information comes from studies performed in archaeological structures and lava flows, since they have recorded snapshots of the past geomagnetic field owing to a thermoremanent magnetization (TRM). These kind of data, named in this work as TRM data, are used to reconstruct the past field (or paleofield) at different spatial scales: from local by determining paleosecular variation (PSV) curves (Cai et al., 2020; Kapper et al., 2020; Molina-Cardín et al., 2018; Osete et al., 2020; Rivero-Montero et al., 2021) to global by using spherical harmonic analysis (Arneitz et al., 2019; Campuzano et al., 2019; Constable et al., 2016). The spatial and temporal distributions
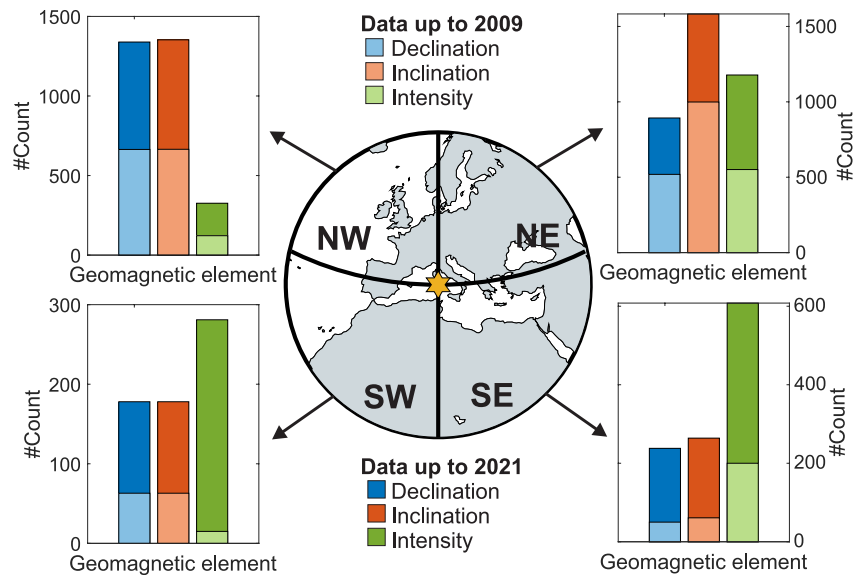
Figure 1. Number of directional (declination and inclination) and intensity data coming from thermoremanent magnetization (TRM) studies in the selected area of interest. Light (dark) colors represent data published before (after) 2009. Blue, red, and green ones are declinations, inclinations, and intensities. The yellow star represents the spherical cap center.

of the TRM data are not homogenous at global scale for the last millennia, and Europe is the continent with the highest amount of data (Brown et al., 2015). Taking advantage of having a high density of data at continent scale, regional reconstructions seem to be the most optimal approach to describe the past geomagnetic field in those regions. This approach has been tested successfully in the last decade: the European regional models for the last 3 kyr (SCHA.DIF.3k, Pavón-Carrasco et al., 2009), and for the period 6000 BC (i.e., Before Christ)–1000 BC (SCHA.DIF.8k, Pavón-Carrasco et al., 2010).

The SCHA.DIF.3k regional model was developed by applying the spherical cap harmonic analysis technique (SCHA, Haines, 1985) to the available archaeomagnetic data collected and published up to the end of 2008. This model can be used to estimate the elements of the geomagnetic field in the European continent, northern Africa and Western Asia. For the last decade, the SCHA.DIF.3k model has been widely used as a tool for archaeomagnetic dating, since one can generate reference PSV curves at the location of the undated archaeological or volcanic site (see Pavón-Carrasco et al., 2011) avoiding the relocation error (Casas & Incoronato, 2007). The ability to have precise archaeomagnetic dating depends on how the archaeomagnetic data constrain the regional paleomagnetic reconstructions. In this context, the acquisition of new archaeomagnetic data will better constrain the past behavior of the geomagnetic field and therefore more precise dating results are expected.

During the last decade (2010–2021), numerous paleomagnetic studies have been performed on archaeological and volcanic samples; now it is appropriate to update the SCHA.DIF.3k regional model. In fact, this is the main objective of this study which is focused on the construction of a new regional model of the past geomagnetic field using all the archaeomagnetic data available in the European continent, northern Africa and Western Asia for the last 4 kyr.

2. Data Selection and Motivation

2.1. Archaeomagnetic Data and Motivation for a New Regional Model

To develop the new regional model, we have used all the TRM data available within a spherical cap of 30° of semi-angle centered at 40°N, 10°E (see Figure 1). The data were extracted from the last version of GEOMAGIA50 database (version v3.4, Brown et al., 2015) updated with new studies not yet included in this database while developing this work (e.g., Rivero-Montero et al., 2021; Tema et al., 2021). The major part

Table 1
Number of TRM Data Used in Our Study

Geomagnetic element	Raw data (Q data)	Final data (Q data)
Declination	2,877 (2,724)	2,672 (2,528)
Inclination	3,632 (2,936)	3,438 (2,755)
Intensity	2,933 (1,047)	2,821 (1,023)
Total	9,442 (6,707)	8,931 (6,306)

The data cover the last 4 kyr and are located inside the spherical cap of Figure 1. The data into brackets correspond to the number of quality data, the so-called Q data (see text for more details).

of the selected data corresponded to archaeomagnetic studies, with a low number of volcanic data coming from Greece, Italy (Aeolian Islands and Sicily), Iceland, Portugal (Azores Islands) and Spain (Canary Islands).

The number of new TRM data has considerably increased since 2009, when the previous regional model for Europe SCHA.DIF.3k was generated. In broad terms, we have around 90% more directional data and 180% more intensities for our area and period of interest. In detail, Figure 1 shows our selected area divided into four different regions (NW, NE, SW, and SE). The major part of the new data corresponded to published studies coming from the Southern European regions. It is important to note the high number of new intensity data published since 2009 representing an increment of around 1,800% and 200% for the SW and SE regions, respectively (see Figure 1).

From the initial database of TRM data we have calculated some statistical parameters to apply a first filter to retain only the most accurate data. Uncertainties for directional and intensity data are commonly given by the angle α_{95} (95% confidence level) and the intensity standard deviation error σ_F (at 1σ), respectively. We have used the expressions of Suttie and Nilsson (2019) to transform the α_{95} into standard errors for declinations and inclinations. The mean values for directional errors (at 1σ) were 3.3° for σ_D and 1.4° for σ_I. The mean intensity error σ_F was 3.6 µT that in terms of percentage error (i.e., $100 \cdot \sigma_F/F$) corresponds to a mean value of 6.5%. We have used the previous directional mean errors and the mean percentage intensity error as thresholds to reject all the data with uncertainties higher than three times these values. In terms of age uncertainty, different methods were used to estimate the age of the TRM data (such as archaeological considerations, stratigraphic comparisons, radiocarbon, among others). The age uncertainty is an important key to provide consistent variations of the paleofield and must be checked with attention (e.g., Shaar et al., 2020). For a reduced number of TRM data, as the case of the construction of a local PSV curve, a detailed revision of the methods used for dating and of age uncertainties can be performed, but the number of data involved in regional or global modeling reaches several thousands of data and this revision is not a straightforward task. Consequently, in our regional model we have directly used the age intervals given in the current version of GEOMAGIA50. More information about this issue is given in the supporting information along with Figure S1 that represents the different dating methods used in the database within the spherical cap. The mean age error was 90 years, and as for data uncertainties, we have rejected all data with age uncertainties higher than three times this mean value. Figure S1 also shows the distribution of both age and data uncertainties for the original data set. When there was no information about these uncertainties in the database or in the original publications (less than the 3% of the database), we have estimated the errors as two times the above mean values. After this first filter, the number of TRM data has been compiled in Table 1.

Figure 2 shows the spatial and temporal distribution of the used TRM data after the first filter (last column in Table 1). As in Figure 1, we have also plotted these distributions for the old data published up to 2009 and used in the previous SCHA.DIF.3k model (light colors in Figure 2). In spatial terms, the major part of the data continues being located in Europe, with very few data available for northern Africa and Western Asia. The temporal histograms show how the directional data are scarce for BC millennia and present higher concentration during the Roman and the Middle Age periods. However, the intensity data are more homogenously distributed in time, with a notable increase in the number of data for the two millennia BC.

As seen in Figures 1 and 2, the number of new data published after 2009 was significant enough to check if a new regional model for Europe should be released. To answer this question, we have compared the new data with the previous regional SCHA.DIF.3k model. The previous model only covers the last 3 kyr and, consequently, we have reduced our time window for the new data set from 1000 BC to 1900 AD in this case study. The comparison was carried out using synthetic data derived from SCHA.DIF.3k model and real data. To get the model data from SCHA.DIF.3k, we generated declination, inclination and intensity in the original ages and locations of the new data set and then, we have calculated the residual as the difference between the model and real data. Figure 3 shows the histograms of these residuals. In addition, residuals between the SCHA.DIF.3k model and the old data set (the data set used in that regional model) were also plotted in the histograms for comparison.
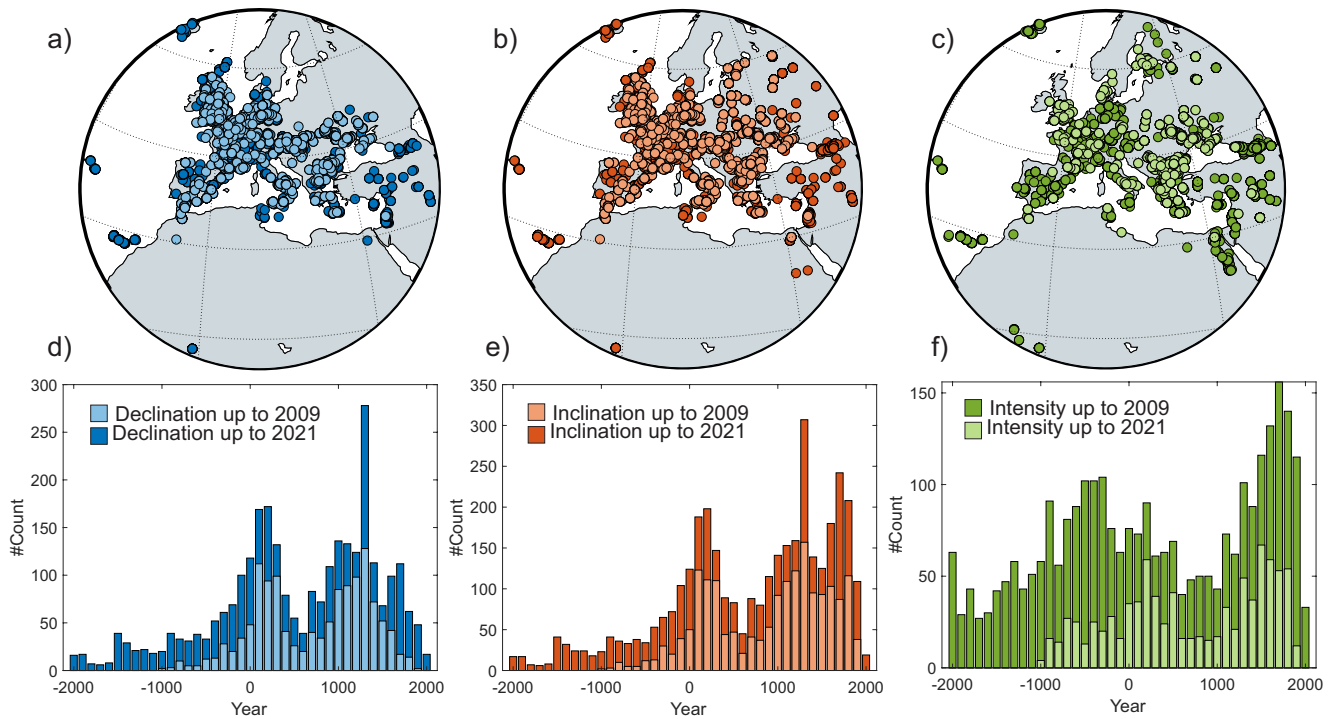
Figure 2. Spatial (upper panel) and temporal (lower panel) distributions for the declination (a and d), inclination (b and e), and intensity (c and f) data. Light colors represent data published up to 2009 and used in the previous model SCHA.DIF.3k.

For directional elements, the histograms of new data were both symmetric with mean values of 0.6° for declinations and 0.9° for inclinations, but they presented higher standard deviations than those given by the histograms using the older data set. The intensity residuals showed a shifted mean value of −3.6 μT and a higher standard deviation than the 2009 intensity data. The higher standard deviations observed for the three geomagnetic elements along with the shift in the mean intensity residuals were clear indicators that the previous regional model SCHA.DIF.3k did not appropriately fit the new database.

In order to illustrate the discrepancy between the new database and the previous SCHA.DIF.3k model, we have plotted the model predictions for the intensity in the Levantine region. We have chosen this location since one of the most important features of the geomagnetic field recorded during the last 4 kyr is the high intensity anomaly located there: the so-called Levantine Iron Age Anomaly (LIAA, Shaar et al., 2017 and references therein). The LIAA is characterized by two short-decadal intensity variations with high values up
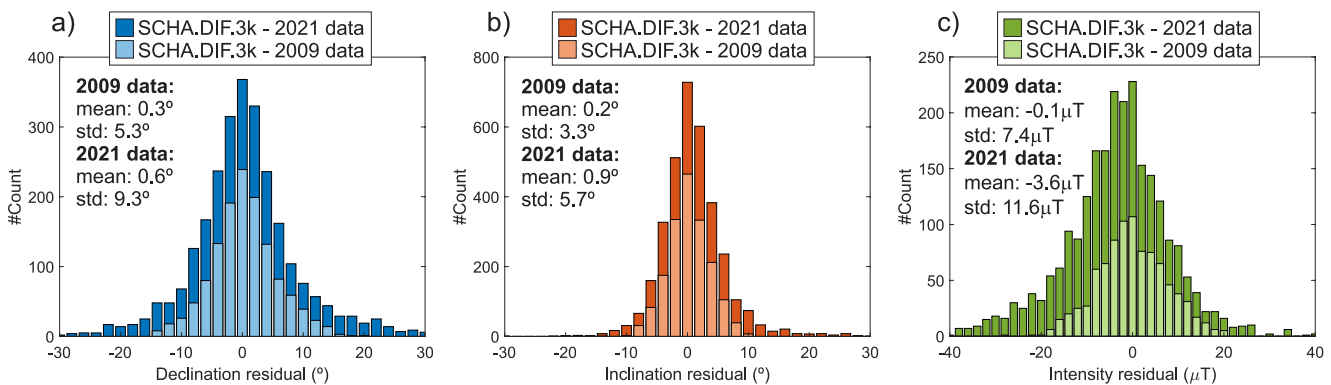

Figure 3. Histograms of the residual data. Declination (a), inclination (b), and intensity (c). Residuals were calculated comparing the SCHA.DIF.3k model with the old database (data published up to 2009, light colors) and the new database (all data published up to 2021, dark colors). Mean and standard deviation values are given in the figure.
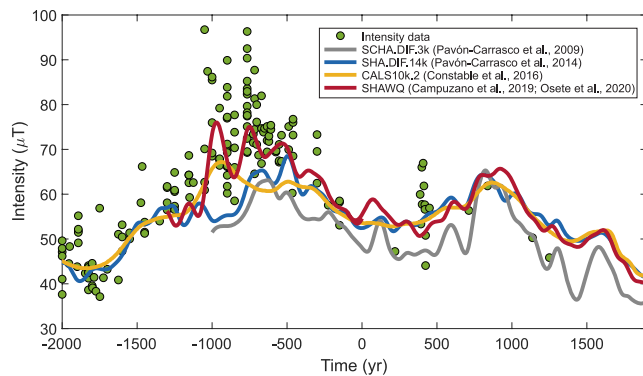
Figure 4. Intensity data of the Levantine region (all data were relocated to common coordinates: 35°N, 35°E). Color curves represent different intensity paleosecular variation (PSV) curves of regional and global models calculated at these coordinates (see legend).

to 100 µT around 950 BC and 700 BC. Figure 4 shows the intensity data for the Levantine area for the last 4 kyr and the SCHA.DIF.3k model prediction (gray curve). All data were relocated by the via-pole method (Noel & Batt, 1990) at common coordinates (35°N, 35°E), where the intensity PSV curve of the regional model was also calculated. The agreement between data and the model is rather poor, especially for the LIAA time interval (1000 BC–500 BC) where the model did not reach the high intensity values. At this point, it is important to mention that the LIAA has been constrained by archaeomagnetic data published after 2009 (Shaar et al., 2017) and therefore this discrepancy was expected.

We have also included in Figure 4 the intensity predictions of a set of different global models recently published (CALS10k.2 of Constable et al., 2016; SCHA.DIF.14k of Pavón-Carrasco et al., 2014a; SHAWQ2k of Campuzano et al., 2019; and SHAWQ-Iron Age of Osete et al., 2020). These global models contain data after 2009 and thus a better agreement between intensity PSV curves calculated from these global models (color curves in Figure 4) and data should be expected. However, most of the global models underestimated the intensity data during the LIAA, with values around 40%–50% lower than those indicated by the two maxima shown in the LIAA. According to all these results, we answered positively the previous question: we need a new regional model to better fit the new data published during the last decade in the European continent and adjacent areas.

2.2. Ranking the Archaeomagnetic and Volcanic Data

Following Campuzano et al. (2019) some of the TRM data within the selected spatial and temporal windows were labeled as Q (quality) data. The criteria to label a TRM data as Q data depend on the statistical parameters and laboratory protocols involved in the data measurement (Chauvin et al., 2000). Here, we have summarized these criteria to select the Q data. In terms of statistic parameters, we have taken into account the number of specimens used to estimate mean directions and intensities. The data uncertainty (α_{95} for directions and σ_F for archaeointensities) decreases when the number of samples increases. In this study, the TRM data with a minimum number of specimens higher than or equal to three were considered as Q data. Note that when the number of specimens was not available, they were considered to be estimated from less than two specimens and thus these data did not fall into the Q data category.

The laboratory protocol only affects the archaeointensity data, since the protocols to measure directions are quite similar and well accepted by the paleomagnetic community. The Q data label was given to the intensity data derived from the Thellier method (Thellier & Thellier, 1959) and its modifications (see Chauvin et al., 2000; Pavón-Carrasco et al., 2014b for more details). Triaxe method also belongs to this category. In addition, the Q data must also include pTRM checks (i.e., the protocol to detect possible mineralogical changes during the laboratory measurements) and corrections by TRM anisotropy effect (when the data are derived from highly anisotropic archaeological objects, such as potteries or ceramics). Since the effect of this kind of anisotropy in volcanic samples is usually low, this correction was not required to label as Q the volcanic data

Finally, the 60% of the intensity Q data presented cooling rate corrections. For the other 40% we applied a cooling rate correction of the 5% of the archaeointensity values (Genevey et al., 2008). In summary, all the intensity TRM data estimated by more than or equal to three specimens and applying the laboratory protocol detailed above were labeled as Q data. For directional data, the Q label was provided to all the declinations and inclinations calculated by three or more specimens. The total number of Q data is given in Table 1 in brackets and a complete list of these data is given in the Table S1.

Since the Q data have passed stricter selection criteria than the rest of the TRM data, they should provide more realistic captures of the past geomagnetic field. Campuzano et al. (2019) have shown that due to the non-homogeneous temporal and spatial distributions of the TRM data at global scale, both type of data (i.e., Q data and the rest of the data) were needed to better constrain the global archaeomagnetic
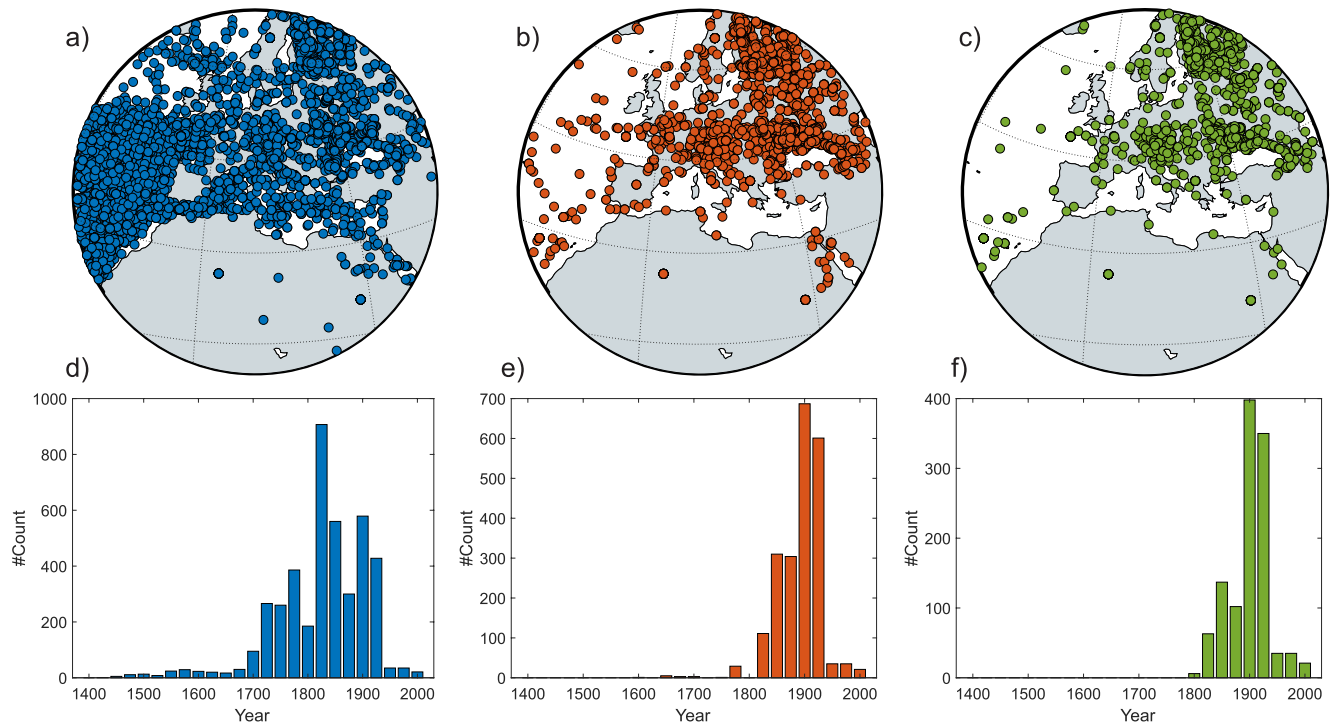
Figure 5. Spatial (upper panel) and temporal (lower panel) distributions of the historical data compiled in HISTMAG database by Arneitz et al. (2017). Declination (column a), inclination (column b), and intensity (column c).

reconstruction SHAWQ2k. However, in our case we can take advantage that Europe and adjacent areas are characterized by the largest density of Q data and we have examined if the number of Q data is enough to provide a robust regional archaeomagnetic reconstruction inside the spherical cap. To do that, we have performed a test study using synthetic data from the geomagnetic model IGRF (Thébault et al., 2015). The objective was to reproduce a constant IGRF model at 1,900 in the time window 2000 BC–1900 AD using the same spatial and temporal distributions of the original Q data. Results (given in the supporting information) were positive and showed that robust regional models can be developed in Europe using only the most reliable data, that is the Q data. Consequently, we have only used the Q data in our study.

2.3. Historical Data

In order to constrain the geomagnetic field behavior inside our spherical cap during the last centuries, we have also included direct measurements as those compiled in the HISTMAG database (Arneitz et al., 2017). HISTMAG allowed us to extract all the historical data available inside the spherical cap of Figure 1. The number of declinations was considerably higher than the other two geomagnetic elements, with historical values measured since the fifteenth century. The spatial and temporal distribution of these data were plotted in Figure 5 following the same color code as Figure 2 for each geomagnetic field element.

For the intensity, some measurements were given by relative intensities or by the horizontal element H. Relative intensities were rejected from our data set, but the horizontal intensities were transformed into absolute intensities using the associated inclination values following the trigonometric expression $F = H / \cos(I)$. The total number of historical data used for the new regional model was 4,242 declinations, 2,098 inclinations, and 1,098 intensities. In terms of weighting, since the historical data provided direct measurements of the past geomagnetic field, we have established for these data a weight three times higher than the Q archaeomagnetic data. We have used this weighting scheme in the modeling approach.

3. Methodology

Taking into account the geometry of our area of interest and that all the data were approximately located at the same altitude, that is the Earth's surface, we have chosen the revised spherical cap harmonic analysis in two dimensions (R-SCHA2D, Thébault, 2008) as the best approach to spatially model the input data. This method was successfully applied to model the past geomagnetic field during the last millennia in Europe (Pavón-Carrasco et al., 2010). Apart from the classical spherical cap harmonic functions, the R-SCHA2D technique involves a new set of basis functions, the Mehler conical functions, that provides a better definition of the geomagnetic field properties within the spherical cap. In Thébault and Gaya-Piqué (2008) readers can find more information about this modeling technique. In terms of R-SCHA2D applied to the geomagnetic field, the general solution of the Laplace equation is expressed by an expansion in terms of spherical cap harmonics and the Mehler functions (we have considered all the data in a geocentric frame at the same distance to the Earth's center, i.e., the average radius of the Earth a = 6,371.2 km) as

$$
\begin{aligned}
V\left(r,\theta,\lambda\right) = a \sum_{k=0}^{K_{\text{int}}} \sum_{m=0}^{k} P_{n_k}^m\left(\cos\theta\right) \cdot \left(g_{n_k}^{m,i} \cos m\lambda + h_{n_k}^{m,i} \sin m\lambda\right) + \\
+ a \sum_{k=0}^{K_{ext}} \sum_{m=0}^{k} P_{n_k}^m\left(\cos\theta\right) \cdot \left(g_{n_k}^{m,e} \cos m\lambda + h_{n_k}^{m,e} \sin m\lambda\right) + \\
+ a \sum_{m\geq 0}^{M} P_{-1/2}^m\left(\cos\theta\right) \cdot \left(G_{-1/2}^m \cos m\lambda + H_{-1/2}^m \sin m\lambda\right).
\end{aligned}
\tag{1}
$$

where θ and λ are the colatitude and the longitude of the data in the cap reference frame. $P_{n_k}{}^m(\cos\theta)$ are associated Legendre functions of real degree n_k and integer order m. $P_{-1/2}{}^m(\cos\theta)$ are a special case of the Mehler functions. $g_{n_k}{}^{m,i-e}$ and $h_{n_k}{}^{m,i-e}$ are the SCH coefficients (Haines, 1985), with the subindex i indicating the internal potential and e the external potential (it is important to note that these coefficients do not have the same meaning as in the Spherical Harmonic Analysis). $G_{-1/2}{}^m$ and $H_{-1/2}{}^m$ are the new coefficients introduced by Thébault (2008).

The new potential in Equation 1 does not include both sets of basis Legendre functions (with $k - m$ even and $k - m$ odd), because the revised version of the SCHA method only takes into account the Legendre functions with $k - m$ even. The other set of basis functions is replaced by the Mehler functions. In order to include the time in Equation 1, we have expressed all the coefficients in a basis function expansions of penalized cubic b-splines with fix knot points within the considered time window.

To jointly model the three geomagnetic field elements, we have used the Fréchet derivative matrix to solve the non-linear relationship between the geomagnetic elements and the SCH coefficients. For the declination (similar for inclination and intensity) we have applied the following expression (see Pavón-Carrasco et al., 2010 for details):

$$
D\left(\vec{m}\right) = D\left(\vec{m}_0\right) + \frac{\partial D\left(\vec{m}\right)}{\partial m} |_{m_0} \cdot \delta\vec{m} = D\left(\vec{m}_0\right) + \widehat{A_D}\left(\vec{m}_0\right) \cdot \delta\vec{m}
\tag{2}
$$

where $D\left(\vec{m}_0\right)$ is an initial value of the declination, $\widehat{A_D}\left(\vec{m}_0\right) = \frac{\partial D\left(\vec{m}\right)}{\partial m} |_{m_0}$ is the Fréchet derivative matrix of the declination expression, and $\delta\vec{m}$ is the vector of the relative SCH coefficients. A regularized weighted least square inversion was applied to estimate the set of SCH coefficients of Equation 1 by means of Equation 2:

$$
\delta\vec{m} = \left(\hat{A}' \cdot \hat{W} \cdot \hat{A} + \alpha \cdot \hat{\Psi} + \tau \cdot \hat{\Phi}\right)^{-1} \hat{A}' \cdot \hat{W} \cdot \vec{\gamma}
\tag{3}
$$

were $\hat{W}$ is the weight matrix, $\hat{\Psi}$ and $\hat{\Phi}$ are matrices representing the spatial and temporal regularization, respectively; and $\vec{\gamma}$ is the vector of input data (i.e., declinations, inclinations and intensities). We have followed Talarn et al. (2017) to obtain the regularization matrices. The spatial roughness $\hat{\Psi}$ was estimated by the square norm of the geomagnetic field within the spherical cap and the temporal regularization $\hat{\Phi}$ was

based on the square of the second time derivative of the radial field at the Earth's surface. α and τ are scalar parameters that were fixed according to the best compromise between model complexity and data misfit. The regularization is a key approach to provide realistic geomagnetic field variation also in areas characterized by a low density of data, such as the case of northern Africa in our spherical cap.

From the input database, Equation 3 provided a set of SCH coefficients. However, we needed to estimate the error of these coefficients to provide robust results. To do that, we have applied a random bootstrap method to transfer the input data uncertainties to the SCH coefficients errors. Using random values taking into account both measure and age uncertainties of each datum, we have created 5,000 different databases from the original database. We have then applied Equation 3 for each database obtaining an ensemble of 5,000 regional models. The final set of SCH coefficients along with the error, was then provided by the mean and standard deviation of the 5,000 ensembles of SCH coefficients.

As defined in Equation 2, initial values for each geomagnetic element must be provided before the inversion approach. We have used as starting model an inclined dipole field calculated from the whole input data. Details about the initial model are given in the supporting information. Using this inclined dipole field model, we have estimated all the initial values of the geomagnetic elements involved in Equation 3.

The regional paleomagnetic reconstruction was developed using the following parameters. The maxima expansion of the spherical cap harmonic degree in Equation 1 were $K_{int} = 3$ for the internal functions (10 SCH coefficients), $K_{ext} = 2$ for the external functions (5 SCH coefficients), and $M = 2$ for the Mehler functions (5 SCH coefficients). According to Thebáult et al. (2006) this expansion is equivalent to a global spherical harmonic expansion of degree ca. 10. The temporal b-splines were homogeneously distributed every 50 years from 2100 BC to 2000 AD. We have included data coming from 100 years before and after the final time window (2000 BC–1900 AD) to avoid temporal boundary effects in the modeling approach. For the 5000-ensemble of regional models, we have used the parameters α and τ equal to $3 \cdot 10^{-4}$ nT^{-2} and $2 \cdot 10^{-3}$ nT^{-2} yr^4, respectively. These damping parameters were chosen according to numerous tests based on the geomagnetic field norm inside the spherical cap and data residuals (see the supporting information for more details).

4. SCHA.DIF.14k Paleomagnetic Reconstruction

4.1. Results and Residual Data

The application of Equation 3 to the input data set provided a set of 20 time-dependent SCH coefficients. The final set of coefficients was derived from the mean and standard deviation of the ensemble of 5,000 regional models. Following our previous studies on regional paleomagnetic reconstructions (Pavón-Carrasco et al., 2009, 2010), we have named the new regional model as SCHA.DIF.4k, where the term SCHA involves the applied approach, DIF means the three paleomagnetic elements (D-declination, I-inclination and F-intensity), and 4k indicates the time interval, that is last 4 kyr. To evaluate the paleomagnetic reconstruction, we have used the root mean square (rms) errors of the three geomagnetic elements and for the two kinds of input data, that is TRM and historical data. The rms errors along with the histograms of the residuals calculated from the difference between the input data and the synthetic values from SCHA.DIF.4k are plotted in Figure 6. As expected, the TRM data presented larger rms errors than the historical data, highlighting the dispersion presented in that kind of data, as can be seen for example in the archaeointensity data plotted in Figure 4. All the histograms followed symmetrical distributions with mean values close to zero. Inclination (intensity) residuals are characterized by the lowest (highest) rms errors for both kinds of data.

4.2. Geomagnetic Field Variations in Europe and Neighboring Areas for the Last four Millennia

Using the SCHA.DIF.4k paleomagnetic reconstruction one can generate synthetic paleomagnetic data at any location inside the spherical cap of Figure 1. Snapshot maps of the three geomagnetic elements from 2000 BC to 1900 AD are represented in Figure 7 (an animation with these maps every 20 years is also available as supporting information). In addition, the SCHA.DIF.4k model is available at http://pc213fis.fis. ucm.es/scha.dif.4k/index.html and http://earthref.org/ERDA/2454/. In these websites, the user can find a
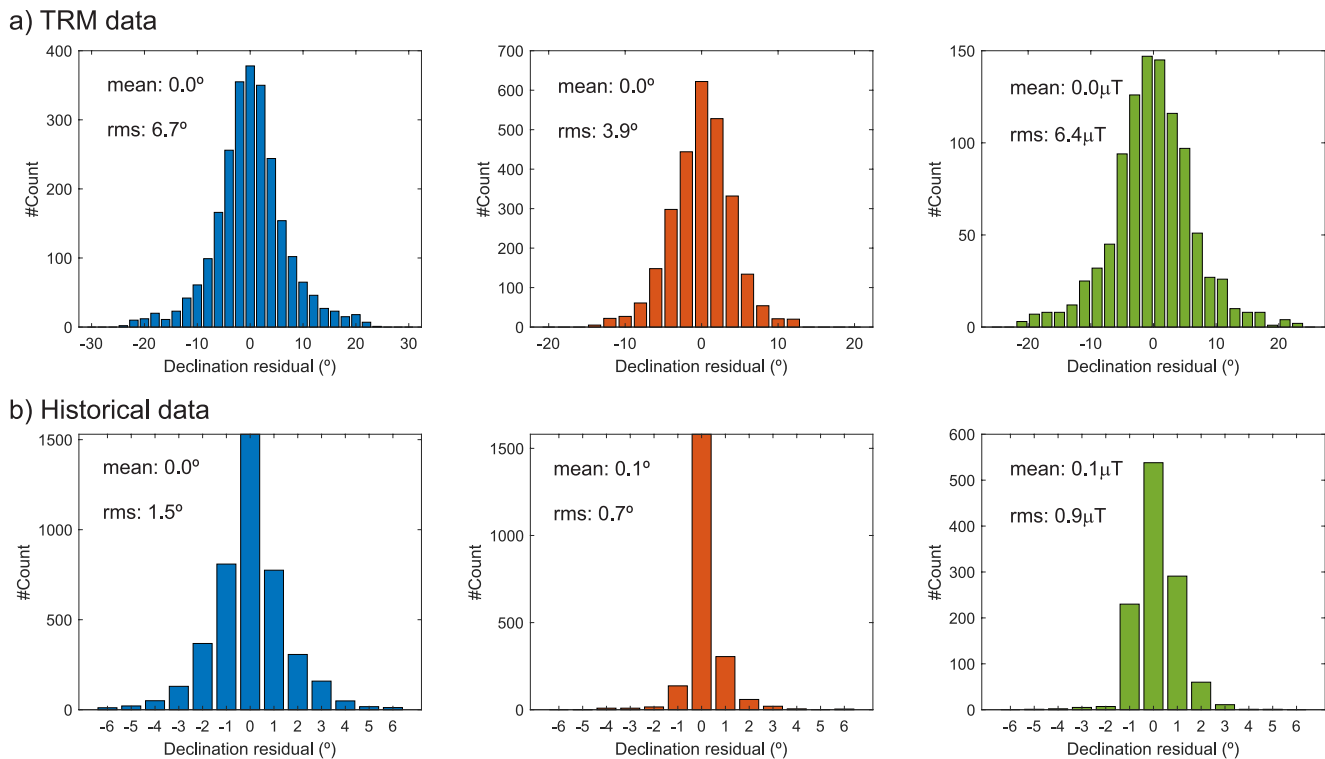
Figure 6. Root mean square (rms) errors and histograms of the residuals for the (a) thermoremanent magnetization (TRM) (archaeomagnetic/volcanic) and (b) historical data. Declinations are represented in the left panel, inclinations in the center panel and intensity in the right panel.

Matlab script to generate PSV curves from 2000 BC to 1900 AD of the declination, inclination and intensity, given a geographical location inside the spherical cap. The script also allows users to download a table with the input data in an area of 800 km of radius from the selected location.

To analyze the behavior of the past geomagnetic field at regional scale, we have represented in Figure 8 PSV curves at two representative locations in Western Europe (40°N, 5°W) and the Middle East (35°N, 35°E). In these figures, the input data within a spherical region of 800 km of radius centered at each location are also plotted after relocation by the via-pole method. For comparison, we have also included the previous SCHA.DIF.3k regional model (green lines) and recent global paleomagnetic reconstructions (see legend in Figure 8). In addition, Figure 8 contains Hovmöller diagrams with the spatial and temporal evolution of the three geomagnetic elements calculated by the SCHA.DIF.4k model along an east-west profile at a constant latitude of 40°N. This kind of diagram is useful to correlate in a single figure some features of the geomagnetic elements, such as the occurrence of maxima and minima, in both space (east to west) and time domains.

4.2.1. Declination Element

For Western Europe (Figure 8a, left), declinations present a high variability with values between 30° east (positive values) and 30° west (negative values). Two maxima are present around 800 BC and 900 AD (maximum eastern declinations) and a minimum around 1800 AD (minimum western declinations). Between 500 BC and 500 AD, Western Europe is characterized by no significant changes in declinations (a plateau) with values close to 0°. This plateau behavior will be a handicap for dating purposes, especially when only directional information is used. For Middle East (Figure 8b, left), declinations show lower amplitudes ranging between ~20° east and 15° west. In more detail, for the second millennium BC, the curve presents a sequence of maxima and minima with a characteristic period of 500 years. The first millennium BC records a maximum around 1000 BC followed by a minimum at 300 BC. For the last two millennia, the declination presents a prominent minimum about 600 AD, a maximum around 1200 AD followed by a minimum at 1750 AD.
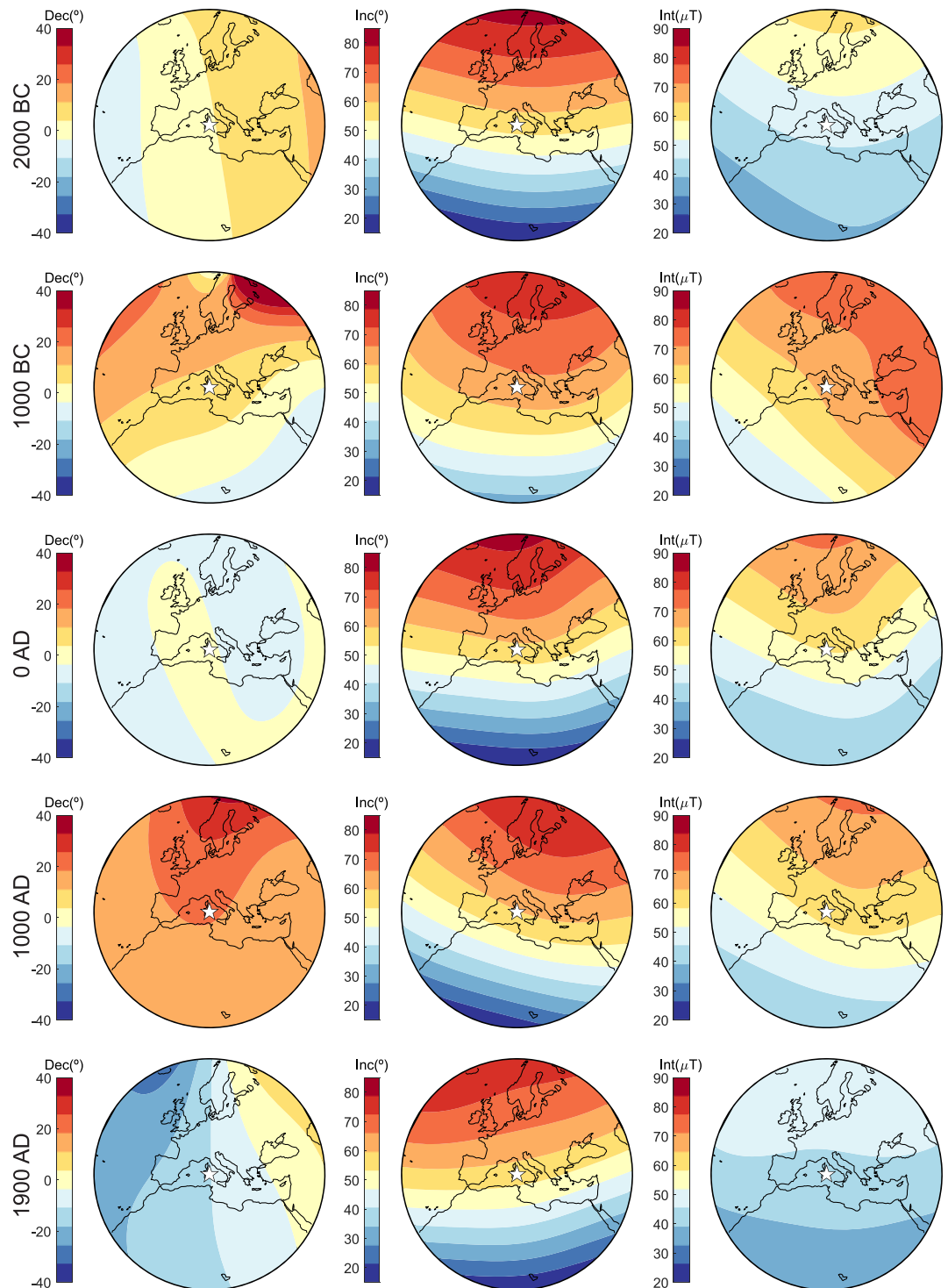
Figure 7. Declination (left), inclination (center), and intensity (right) maps by the SCHA.DIF.4k model. Maps at 2000 BC, 1000 BC, 0 AD, 1000 AD, and 1900 AD. The white star indicates the center of the spherical cap.

According to the Hovmöller diagram (Figure 8c, left) and the animated maps of the supporting information, the eastern maximum around 1000 BC is observed around 800 BC in Western Europe characterized by higher eastern declinations. This maximum is well-constrained by new declination data from West-Central Europe (Osete et al., 2020; Schnepp et al., 2020). In the first millennium AD there is a noticeable sharp minimum in the eastern curve around 600 AD that expands to west up to 10°E of longitudes. The highest
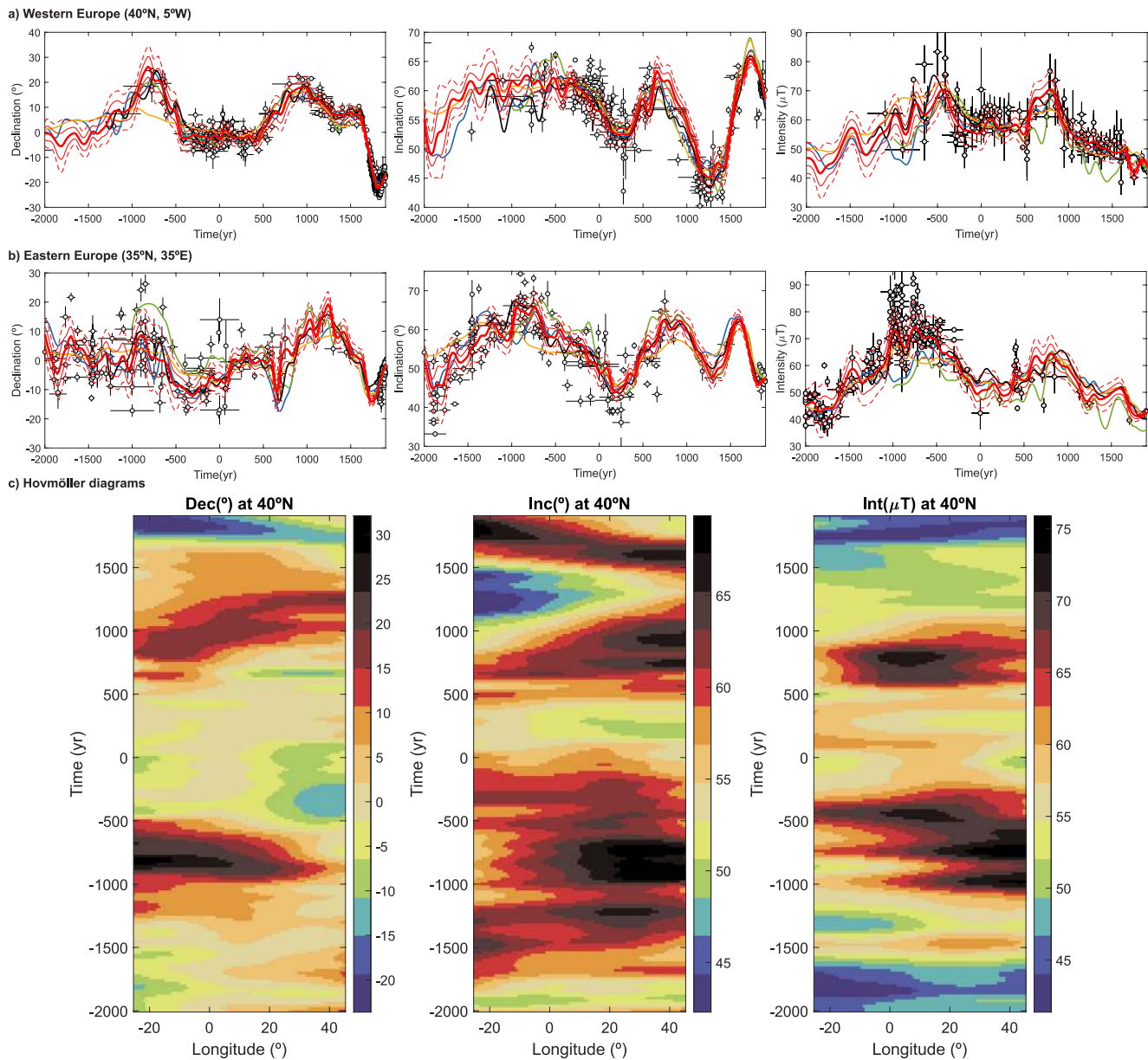
Figure 8. Paleosecular variation (PSV) curves at (a) 40°N, 5°W and (b) 35°N, 35°E coordinates, and (c) Hovmöller diagrams for the declination (left), inclination (center), and intensity (right) elements. For the PSV curves: red curves correspond to the new SCHA.DIF.4k model with error bands at 1σ (thin red lines) and 2σ (dashed red lines). Green curves represent the previous regional archaeomagnetic model SCHA.DIF.3k. In addition, global archaeomagnetic models CALS10k.2 (yellow curves), SHA.DIF.14k (blue curves) and SHAWQ family (black curves) are also plotted. Archaeomagnetic and historical data referred to each location are plotted for comparison as gray dots (with error bars). For the Hovmöller diagrams: they are calculated at a constant latitude of 40°N for the range of longitudes inside the spherical cap.

east declination maxima (such as a double oscillation) in the eastern curve for the last two millennia (1000 AD and 1250 AD) are observed around 300 years before in Western Europe. Finally, the Hovmöller shows the well-known westward drift of the declination for the instrumental period, with minimum declination values moving from east to west during the last four centuries.

4.2.2. Inclination Element

The inclination curves show similar behavior in the entire European continent. Three characteristic maxima are recorded in Western Europe (Figure 8a, center) around 1250 BC (not well constrained), 600 AD and 1800 AD. These three maxima are preceded by minimum values around 1850 BC, 250 AD and 1250 AD,

respectively. An inclination plateau characterizes the paleofield between 1000 BC and 200 BC. The Middle East curve (Figure 8b, center) also provides different maxima (1200 BC, 1000 BC, 700 BC, 800–900 AD, and 1600 AD) but at different times with respect to Western Europe. However, the eastern inclination minima seem to occur at the same time as those of the western side, with an exception of the first one, which is well constrained by inclination data around 1900 BC.

Following the Hovmöller diagram (Figure 8c, center) and the animated maps, the first eastern maximum around 1200 BC seems to be correlated with the maximum of Western Europe around 1250 BC. However, the maxima observed around 1000 BC and 700 BC show a vanished westward continuation. Here, it is worth mentioning that recent archaeomagnetic studies from Middle East (Shaar et al., 2017 and references therein) indicate that these high inclination values around 1,000–700 BC are correlated with the intensity LIAA event. During the millennia AD, there are similar features from East to West of Europe: the maximum around 600 AD and the minimum around 1250 AD are observed in the entire longitudinal profile. The eastern maximum around 950 AD is only presented in the eastern side. Finally, as for declinations, the inclination shows a clear maximum with a westward drift during the instrumental period (1,600–1,900).

4.2.3. Intensity Element

The intensity curves show a common long-trend behavior in Western Europe and in the Middle East (Figures 8a and 8b, right panels, respectively), with important maxima during the first millennium BC and the second half of the first millennium AD. The PSV curves, the Hovmöller (Figure 8c, right) and the animated maps (supporting information) help to analyze the spatial and temporal behavior of these maxima. In Western Europe, there are two maxima around 700 BC and 500 BC which are in agreement with recent studies from this European side (Osete et al., 2020). There are two previous maxima with lower amplitude around 1500 BC and 1000 BC that are not well constrained by the data. In fact, due to the lack of Q data in Central and Western Europe for this time, these western maxima could be a direct influence of the higher maxima at 1500 BC and 1000 BC of the Middle East. As suggested by previous studies (Genevey et al., 2016; Gómez-Paccard et al., 2016; Schnepp et al., 2020), the next prominent maximum in the western curve occurs at 800 AD followed by a continuous intensity decay up to the present days.

In the Middle East, the first and highest maximum occurs around 1000 BC and its amplitude decreases rapidly toward Western Europe (see Hovmöller). This eastern maximum defines the beginning of the LIAA event (Ertepinar et al., 2020; Rivero-Montero et al., 2021; Shaar et al., 2017), one of the most important features of the past geomagnetic field. The Hovmöller diagram indicates that the LIAA event begins around 1000 BC at eastern longitudes (20°–40°E) whose amplitude vanishes westwards. The animation maps show this maximum as an important intensity region that increases and decreases in situ (between 1000 BC and 940 BC). Due to the limitation of the SCHA.DIF.4k model, no information about the LIAA can be provided toward Asia. After this maximum, other eastern maximum around 750 BC seems to constrain the LIAA. However, this maximum extends more westwards and is not observed as an isolated intensity patch in the animated maps. Finally, the next maximum around 550 BC is observed during the same time for all the longitudinal profile, indicating an intensity feature of the Earth's magnetic field at continental scale (see also the intensity animation maps between 600 BC and 400 BC).

Finally, during the second half of the first millennium AD, the intensity shows a clear maximum in Europe, with a double oscillation in Eastern Europe (Kovacheva et al., 2014). This double oscillation has been also recorded by archaeointensity data from Central-Western Europe (Genevey et al., 2016; Gómez-Paccard et al., 2016), but more data are needed to better constrain this double oscillation in this European side. After 1000 AD, all Europe is characterized by an intensity decrease trend up to the instrumental period (ca. 1,840 for intensities).

The new SCHA.DIF.4k regional model has been compared with the previous SCHA.DIF.3k regional model at the same west and east locations (Figures 8a and 8b). As expected, the new regional model fits better to the data than the previous SCHA.DIF.3k model. Both the new data published after 2009 and the use of the Q data are responsible of this improvement. In addition, the new model also provides information of the paleofield during the second millennium BC. In Western Europe, the previous model underestimates the intensities providing lower values than those depicted by the data. In Eastern Europe, the discrepancy is more noticeable: apart from the underestimation of intensities, the previous regional model overestimates the declinations and inclinations during the first millennium BC in this region.

Table 2
RMS Errors for the TRM (Only Q Data) and Historical Data for Different Paleomagnetic Reconstructions

Model	Archaeomagnetic and volcanic data			Historical data		
	RMS Dec (°)	RMS Inc (°)	RMS Int (µT)	RMS Dec (°)	RMS Inc (°)	RMS Int (µT)
SCHA.DIF.4k	6.7	3.9	6.4	1.5	0.7	0.9
SHA.DIF.14k	7.3	4.0	9.4	1.7	0.7	1.1
CALS10k.2	7.8	4.2	8.9	1.7	0.7	0.9
SHAWQ family	7.2	3.8	7.5	3.4	0.9	1.0

Abbreviation: RMS, root mean square.

The new regional model is also compared with previous global paleomagnetic reconstructions. The CALS10k.2 presents a smoother behavior (more notable in the directional elements in both western and eastern region) due to the use of sedimentary data. The SHA.DIF.14k model presents higher discrepancies for the two millennia BC due to the very low number of archaeomagnetic data available for this period when this global reconstruction was generated, in 2013. In fact, for the eastern location, the SHA.DIF.14k model does not record the intensity anomaly of the LIAA because these data were published after the model generation.

It is worth noting that the most recent reconstructions, the SHAWQ global models, provide similar paleofield variations as the new SCHA.DIF.4k regional model. This agreement was expected because the criteria used in the regional model to select the Q data was similar to that used for the SHAWQ global models. The SHAWQ family models used the whole database to have a better spatial and temporal coverage providing different weights for the Q data and the rest of the data (see Campuzano et al., 2019). The SCHA.DIF.4k model only involves Q data and thus, it is reasonable that there is good general agreement between both reconstructions. However, some differences must be pointed out: (1) new recent Q data, published during 2020 and 2021, have been included in the regional model and thus were not used in the SHAWQ family models. (2) The historical data were not used in the global SHAWQ reconstructions, so the regional model provides more reliable estimations of the geomagnetic elements for the historical periods. (3) In the SHAWQ family, the intensity data without cooling rate estimations were not corrected. (4) The new regional model covers the last 4,000 years, that is 700 years longer than the global paleoreconstruction.

To quantify the improvement reached with the new regional model for Europe compared to the global models, we have calculated the rms errors from data and models. The rms error is calculated for both TRM (only Q data) and historical data (see Table 2). Results show that, at overall, the lowest rms errors are reached by using the SCHA.DIF.4k model. Similar results are found for the SHAWQ global model, but as indicated above, this global model was not constrained by historical data and this is reflected by the higher rms declination error (more than twice the rms of the SCHA.DIF.4k model) for the historical data.

4.3. Application to Archaeomagnetic Dating

The new regional paleomagnetic reconstruction SCHA.DIF.4k can be used in the archaeo_dating tool developed by Pavón-Carrasco et al. (2011), a Matlab interface software for archaeomagnetic dating based on the statistical background given by Lanos (2004). This tool establishes a statistical comparison (in terms of probability density functions, PDF) between an undated paleomagnetic data collected in an archaeological or volcanic site and a PSV curve synthetized by the SCHA.DIF.4k model at the same location, avoiding the effect of the relocation error in the dating process (see Pavón-Carrasco et al., 2011 for more details).

The precision of an archaeomagnetic dating is difficult to evaluate, since it depends on several factors. On the one hand, the measurement error of the undated paleomagnetic data plays an important role in the dating process: higher errors provide larger dating uncertainties. On the other hand, the synthetic PSV curves used for dating are key to provide well constrained dates. The characteristics of the data set involved in the paleomagnetic reconstruction and the behavior of the geomagnetic field itself (amplitude and time variability of the geomagnetic elements) also define the precision in archaeomagnetic dating.

We have estimated the dating precision of the new regional model SCHA.DIF.4k using different synthetic PSV curves inside the spherical cap. The method was that given in Pavón-Carrasco et al. (2011), where the synthetic curves represent the geomagnetic field variations and the undated datum is exactly characterized by the values predicted by the curves. To provide a more realistic scenario, the uncertainty of the undated data was increased from 0 to a maximum value. For direction the α_{95} was 0°, 1°, 2°, 3°, 4° while for intensities, we used σ_F values of 0, 1, 2, 3, 4 µT. We have chosen five locations representing the west (40°N, 5°W), north (55°N, 10°E), and center (40°N, 10°E) of Europe, the Middle East (35°N, 35°E), and north of Africa (25°N, 10°E). For each location we have synthetized the curves from the SCHA.DIF.4k model and then we have applied the archaeo_dating tool using synthetic undated data obtained from the same curves and with the increasing uncertainties defined above. It is worth noting that this calculation does not mean that lower age uncertainties could not be reached at one individual dating site. This would be the case, for example, of magnetic data that fall within highly variable segments of the master curve, which can be dated more precisely than the ones falling within the non-variable (plateau) segments. We have carried out two different types of dating, first using only the directional information since it is the most common archaeomagnetic dating carried out for the paleomagnetic community due to the facility to measure the directional field. Second, using the full vector, i.e. including the intensity information.

Results, in terms of the semi-amplitude of the archaeomagnetic dating (considered here as the dating precision) given in years, are plotted in Figure 9. For each location, we have plotted the dating precision obtained for a given data uncertainty scenario. Note that the label "err-0,1,2,3,4" in the legend of Figure 9 indicates the value of the uncertainties, that is err-X means X° for α_{95} and XµT for σ_F. The dating precision depends on four general factors:

(A) The uncertainty of the undated data. As expected, higher uncertainties provide larger dating precisions. In average, the dating precision for the case err-4 (around 150 years) is three times that obtained for the case err-0 (around 50 years)

(B) The temporal data distribution. For all the cases, the dating precision from the two millennia BC are higher due to the low number of data for this time period (see Figure 2)

(C) The behavior of the geomagnetic field itself. The European plateaus shown by declinations between 500 BC and 500 AD and intensities between 300 BC and 500 AD (see Figure 8) contribute to large dating precisions as reflected by the different panels of Figure 9. Contrarily, rapid variations of the geomagnetic elements contribute to improving the dating, this is the case of the fast inclination decay in 700 AD–1200 AD followed by a rapid increase up to 1600 AD

(D) The use of the full vector instead of the directional information only. The use of the full geomagnetic vector (right column in Figure 9) instead of the directional information (left column in Figure 9) constrains better the archaeomagnetic dating, with a general age interval reduction of about 30%. This reduction is noticeable for north Europe (Figure 9d) or high latitude regions, where the high inclinations provide larger declination errors and thus the dating error increases when the direction elements are only used

Finally, we have presented two case studies of archaeomagnetic dating using the full geomagnetic vector, that is declination, inclination and intensity, from two archaeological sites studied by Kovacheva et al. (2004). We have chosen these sites because they represent Eastern and Western Europe. The first example is an archaeomagnetic study carried out in Serdica (Bulgaria) and the second case was focused on an archaeological kiln in Reinach (Switzerland). For the two cases there is a good agreement between the archaeomagnetic dating obtained with the SCHA.DIF.4k model and the archaeological information indicated in the original publication (see Figure 10). For Serdica, the archaeomagnetic model estimated a possible age between 566 and 612 AD (95% of probability) and the archaeological considerations showed similar time interval (565–578 AD). For Reinach, the archaeomagnetic date was constrained between 730 and 827 AD, improving noticeably the archaeological information that only was able to indicate that the archaeological structure belonged to the postroman period. Although in the above cases the results were positive, it is important to highlight some limitations on the use of the SCHA.DIF.4k model as a dating tool. Caution must be taken for dating in regions with a low density of archaeomagnetic data since the model predictions could be not precise. In addition, if the undated data recorded the geomagnetic field elements during a time period characterized by rapid variations, the regional model could be too smooth to provide an accurate dating (see Pavón-Carrasco et al., 2011).
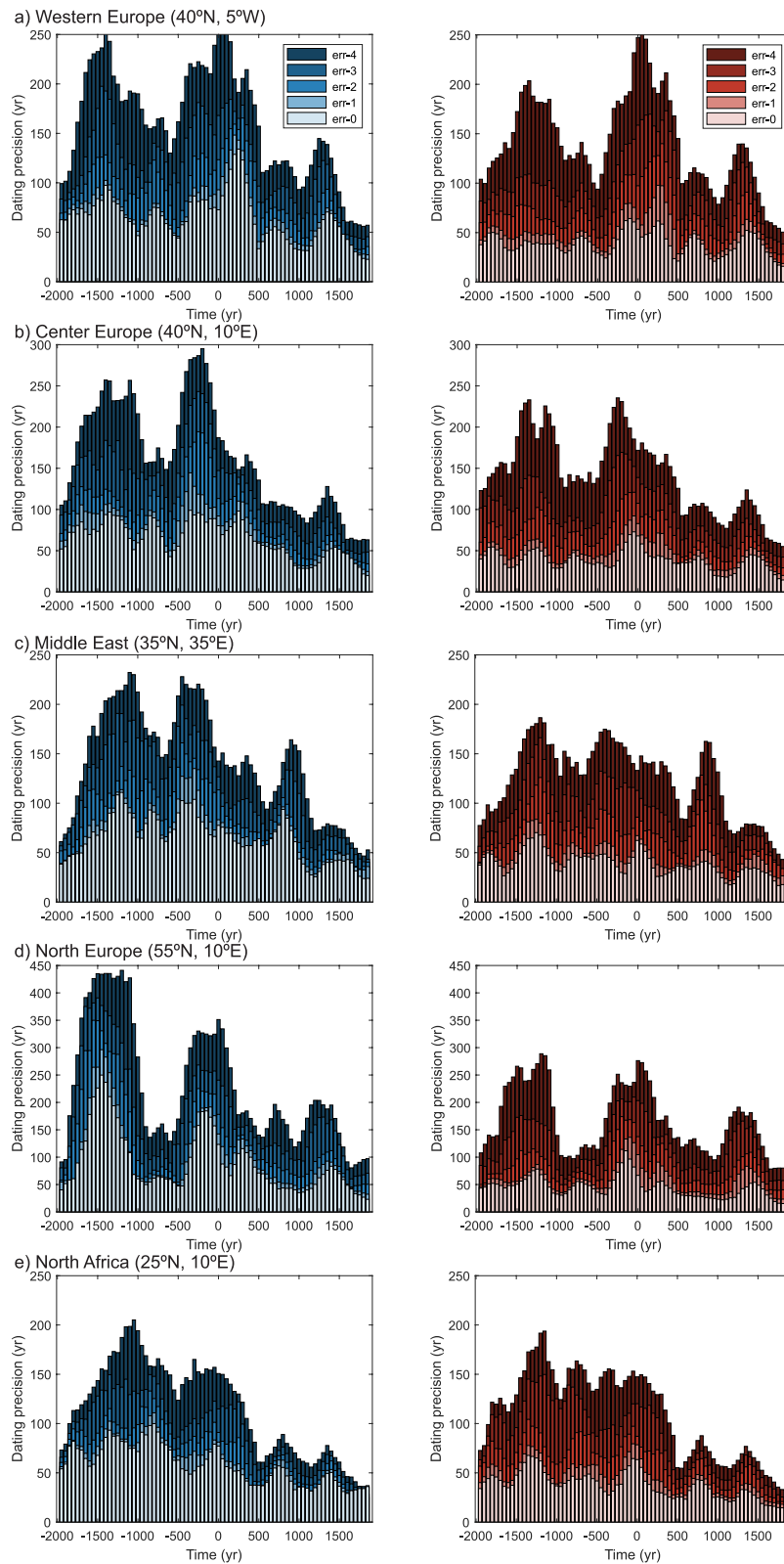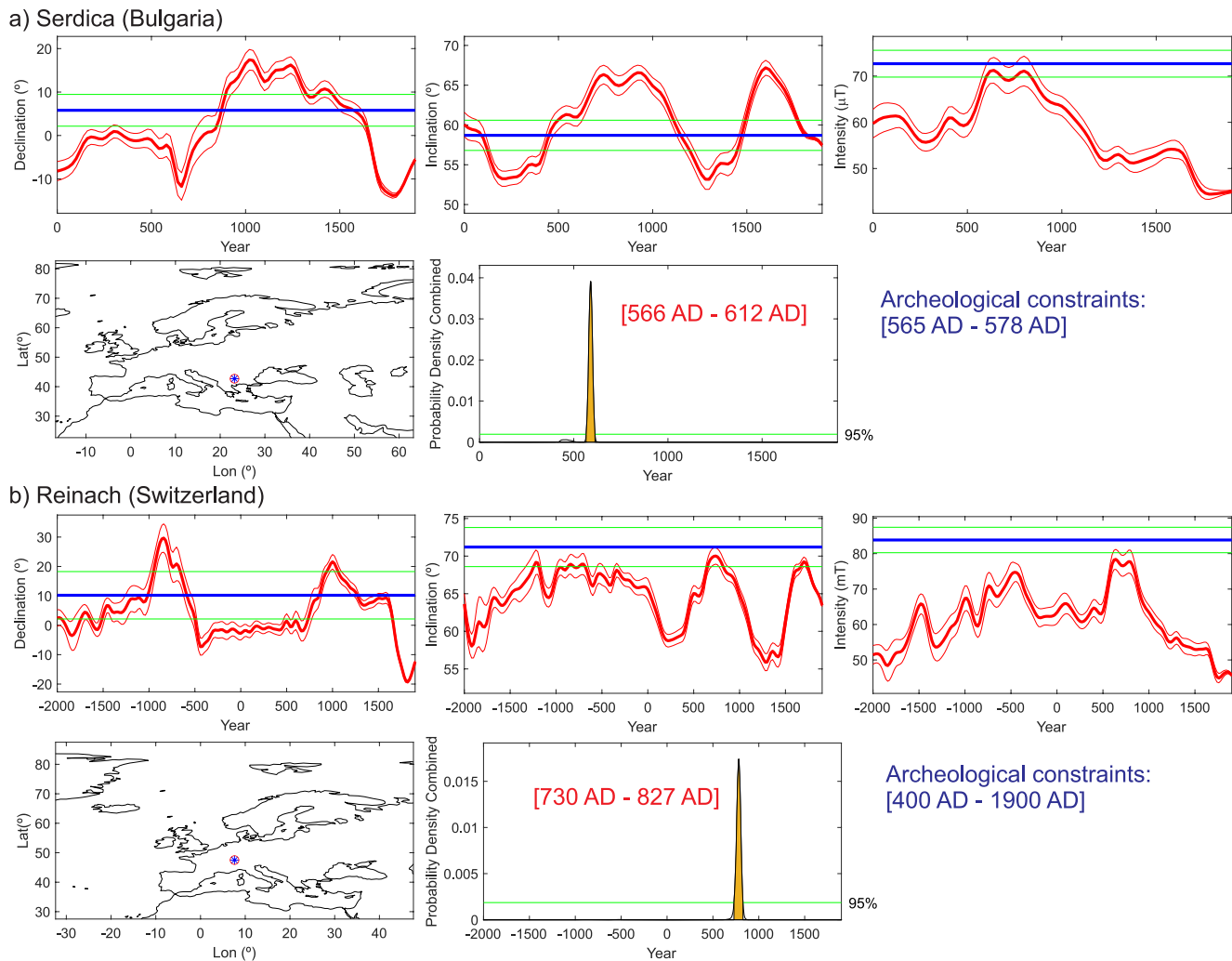
Figure 10. Archaeomagnetic dating of two archaeological structures in (a) Bulgaria and (b) Switzerland using the SCHA.DIF.4k model. Each panel represents the final screen output of the archaeo_dating tool. Top: master paleosecular variation (PSV) curves (red curves with red error bands) of the declination (left), inclination (center) and intensity (right) and the undated archaeomagnetic data (blue line with green error bands). Bottom: regional map (left) with the data location (red point) and the master PSVC location (blue square); combined PDF (center) filled by yellow color and marked with the green threshold line of probability; and the archaeomagnetic dating information in red. In blue, the archaeological constrains of the structures given in the original publications.

5. Conclusion

Thanks to the great effort made by the international paleomagnetic/archaeomagnetic community, the number of archaeomagnetic data is continuously increasing. During the last 10 years, we have 90% more directional and 180% more intensity data in the European continent. Taking advantage of this, we have proposed an updated version of the European regional model SCHA.DIF.3k (published in 2009) covering the last 4 kyr and using only the most reliable archaeomagnetic and volcanic data, the so-called Q data. The new regional reconstruction, SCHA.DIF.4k, provides the geomagnetic field elements (declination, inclination, and intensity) and their uncertainties at any location inside the spherical cap. Model uncertainties are estimated by bootstrapping the data during the inversion process. The new model shows a more robust variation of

Figure 9. Dating precision at 95% confidence (semi-amplitude of the archaeomagnetic dating) for the last four millennia estimated according to the SCHA. DIF.4k model for different locations. The dating precisions were calculated using the archaeo_dating tool with undated data provided by the paleosecular variation (PSV) curves. To provide different dating scenarios, the data uncertainty is increased from 0° to 4° for α_{95} and from 0 to 4 μT for σ_F (in the legend, err-X means X° for α_{95} and XμT for σ_F). Left column represents the dating precision for directional dating (only declination and inclination) and the right column corresponds to dating precision when using the full vector (i.e., declination, inclination, and intensity). See text for details.

the geomagnetic field in Europe, showing how some features can be correlated in both spatial and temporal domains over the entire European continent. This is the case of the LIAA event: the SCHA.DIF.4k model shows this intensity feature around 1000 BC located in Eastern Europe with amplitude fading toward Western Europe. Finally, the new model can be included in the software archaeo_dating to provide a useful tool for archaeological and volcanic dating. In terms of dating, we have performed a case study to evaluate the dating precision using the SCHA.DIF.4k model. Results show that the archaeomagnetic dating are clearly biased by the uncertainty of the data, the evolution of the geomagnetic field itself, and the temporal and spatial distribution of the current European database. In addition, the use of the full geomagnetic vector provides better constrained dates (in average about 50–150 years for the last millennia), reducing in around 30% the date uncertainty with respect to when only the directional information is used. Finally, the new regional archaeomagnetic reconstruction has been used to date two archaeological structures in Western (Switzerland) and Eastern (Bulgaria) Europe.

Data Availability Statement

All the paleomagnetic and historical geomagnetic data used in this work are included in the databases GEOMAGIA50 (https://geomagia.gfz-potsdam.de/), HISTMAG (https://cobs.zamg.ac.at/data/index.php/en/data-access/histmag), and the final data set of Q data is provided as a table in the supporting information.

References

Arneitz, P., Egli, R., Leonhardt, R., & Fabian, K. (2019). A Bayesian iterative geomagnetic model with universal data input: Self-consistent spherical harmonic evolution for the geomagnetic field over the last 4000 years. *Physics of the Earth and Planetary Interiors*, *290*, 57–75. https://doi.org/10.1016/j.pepi.2019.03.008

Arneitz, P., Leonhardt, R., Schnepp, E., Heilig, B., Mayrhofer, F., Kovacs, P., et al. (2017). The HISTMAG database: Combining historical, archaeomagnetic and volcanic data. *Geophysical Journal International*, *210*(3), 1347–1359. https://doi.org/10.1093/gji/ggx245

Brown, M. C., Donadini, F., Korte, M., Nilsson, A., Korhonen, K., Lodge, A., et al. (2015). GEOMAGIA50. v3: 1. General structure and modifications to the archeological and volcanic database. *Earth Planets Space*, *67*, 83. https://doi.org/10.1186/s40623-015-0232-0

Cai, S., Tauxe, L., Wang, W., Deng, C., Pan, Y., Yang, L., & Qin, H., 2020. High-fidelity archeointensity results for the late neolithic period from central China. *Geophysical Research Letters*, *47*(10), e2020GL087625. https://doi.org/10.1029/2020GL087625

Campuzano, S. A., Gómez-Paccard, M., Pavón-Carrasco, F. J., & Osete, M. L. (2019). Emergence and evolution of the South Atlantic anomaly revealed by the new paleomagnetic reconstruction SHAWQ2k. *Earth and Planetary Science Letters*, *512*, 17–26.

Casas, L., & Incoronato, A. (2007). Distribution analysis of errors due to relocation of geomagnetic data using the 'Conversion via Pole' (CVP) method: Implications on archaeomagnetic data. *Geophysical Journal International*, *169*(2), 448–454.

Chauvin, A., Garcia, Y., Lanos, P., & Laubenheimer, F. (2000). Paleointensity of the geomagnetic field recovered on archaeomagnetic sites from France. *Physics of The Earth and Planetary Interiors*, *120*, 111–136.

Constable, C., Korte, M., & Panovska, S. (2016). Persistent high paleosecular variation activity in southern hemisphere for at least 10 000 years. *Earth and Planetary Science Letters*, *453*, 78–86.

Ertepinar, P., Hammond, M. L., Hill, M. J., Biggin, A. J., Langereis, C. G., Herries, A. I. R., et al. (2020). Extreme geomagnetic field variability indicated by Eastern Mediterranean full-vector archaeomagnetic records. *Earth and Planetary Science Letters*, *531*, 115979.

Genevey, A., Gallet, Y., Constable, C. G., Korte, M., & Hulot, G. (2008). ArcheoInt: An upgraded compilation of geomagnetic field intensity data for the past ten millennia and its application to the recovery of the past dipole moment. *Geochemistry, Geophysics, Geosystems*, *9*, Q0438. https://doi.org/10.1029/2007GC001881

Genevey, A., Gallet, Y., Jesset, S., Thébault, E., Bouillon, J., Lefèvre, A., & Le Goff, M. (2016). New archeointensity data from French early medieval pottery production (6th–10th century AD). Tracing 1500 years of geomagnetic field intensity variations in Western Europe. *Physics of the Earth and Planetary Interiors*, *257*, 205–219.

Gómez-Paccard, M., Osete, M. L., Chauvin, A., Pavón-Carrasco, F. J., Pérez-Asensio, M., Jiménez, P., & Lanos, P. (2016). New constraints on the most significant paleointensity change in Western Europe over the last two millennia. A non-dipolar origin? *Earth and Planetary Science Letters*, *454*, 55–64.

Haines, G. V. (1985). Spherical cap harmonic analysis. *Journal of Geophysical Research*, *90*(B3), 2583–2591. https://doi.org/10.1029/JB090iB03p02583

Kapper, L., Serneels, V., Panovska, S., Ruíz, R. G., Hellio, G., de Groot, L., et al. (2020). Novel insights on the geomagnetic field in West Africa from a new intensity reference curve (0-2000 AD). *Scientific Reports*, *10*(1), 1–15.

Kovacheva, M., Hedley, I., Jordanova, N., Kostadinova, M., & Gigov, V. (2004). Archaeomagnetic dating of archaeological sites from Switzerland and Bulgaria. *Journal of Archaeological Science*, *31*(10), 1463–1479.

Kovacheva, M., Kostadinova-Avramova, M., Jordanova, N., Lanos, P., & Boyadzhiev, Y. (2014). Extended and revised archaeomagnetic database and secular variation curves from Bulgaria for the last eight millennia. *Physics of The Earth and Planetary Interiors*, *236*, 79–94.

Lanos, P. (2004). Bayesian inference of calibration curves: Application to archaeomagnetism. In *Tools for constructing chronologies* (pp. 43–82). London: Springer.

Molina-Cardín, A., Campuzano, S. A., Osete, M. L., Rivero-Montero, M., Pavón-Carrasco, F. J., Palencia-Ortas, A., et al. (2018). Updated Iberian archeomagnetic catalogue: New full vector paleosecular variation curve for the last three millennia. *Geochemistry, Geophysics, Geosystems*, *19*, 3637–3656. https://doi.org/10.1029/2018GC007781

Noel, M., & Batt, C. M. (1990). A method for correcting geographically separated remanence directions for the purpose of archaeomagnetic dating. *Geophysical Journal International*, *102*(3), 753–756.

Osete, M. L., Molina-Cardín, A., Campuzano, S. A., Aguilella-Arzo, G., Barrachina-Ibañez, A., Falomir-Granell, F., et al. (2020). Two archaeomagnetic intensity maxima and rapid directional variation rates during the Early Iron Age observed at Iberian coordinates. Implications on the evolution of the Levantine Iron Age Anomaly. *Earth and Planetary Science Letters*, *533*, 116047.

Panovska, S., Korte, M., & Constable, C. G. (2019). One hundred thousand years of geomagnetic field evolution. *Reviews of Geophysics*, *57*, 1289–1337. https://doi.org/10.1029/2019RG000656

Pavón-Carrasco, F. J., Gómez-Paccard, M., Hervé, G., Osete, M. L., & Chauvin, A. (2014b). Intensity of the geomagnetic field in Europe for the last 3 ka: Influence of data quality on geomagnetic field modeling. *Geochemistry, Geophysics, Geosystems*, *15*, 2515–2530. https://doi.org/10.1002/2014GC005311

Pavón-Carrasco, F. J., Osete, M. L., & Torta, J. M. (2010). Regional modeling of the geomagnetic field in Europe from 6000 to 1000 BC. *Geochemistry, Geophysics, Geosystems*, *11*. https://doi.org/10.1029/2010GC003197

Pavón-Carrasco, F. J., Osete, M. L., Torta, J. M., & De Santis, A. (2014a). A geomagnetic field model for the Holocene based on archaeomagnetic and lava flow data. *Earth and Planetary Science Letters*, *388*, 98–109.

Pavón-Carrasco, F. J., Osete, M. L., Torta, J. M., & Gaya-Piqué, L. R. (2009). A regional archaeomagnetic model for Europe for the last 3000 years, SCHA.DIF.3K: Applications to archaeomagnetic dating. *Geochemistry, Geophysics, Geosystems*, *10*(3), Q03013. https://doi.org/10.1029/2008GC002244

Pavón-Carrasco, F. J., Rodríguez-González, J., Osete, M. L., & Torta, J. M. (2011). A Matlab tool for archaeomagnetic dating. *Journal of Archaeological Science*, *38*(2), 408–419.

Rivero-Montero, M., Gómez-Paccard, M., Kondopoulou, D., Tema, E., Pavón-Carrasco, F. J., Aidona, E., et al. (2021). Geomagnetic field intensity changes in the Central Mediterranean between 1500 BCE and 150 CE: Implications for the Levantine Iron Age Anomaly evolution. *Earth and Planetary Science Letters*, *557*, 116732.

Schnepp, E., Thallner, D., Arneitz, P., & Leonhardt, R. (2020). New archeomagnetic secular variation data from Central Europe, II: Intensities. *Physics of the Earth and Planetary Interiors*, *309*.106605.

Schnepp, E., Thallner, D., Arneitz, P., Mauritsch, H., Scholger, R., Rolf, C., & Leonhardt, R. (2020). New archeomagnetic secular variation data from Central Europe. I: Directions. *Geophysical Journal International*, *220*(2), 1023–1044.

Shaar, R., Bechar, S., Finkelstein, I., Gallet, Y., Martin, M. A. S., Ebert, Y., et al. (2020). Synchronizing geomagnetic field intensity records in the Levant between the 23rd and 15th centuries BCE: Chronological and methodological implications. *Geochemistry, Geophysics. Geosystems*, *21*, e2020GC009251. https://doi.org/10.1029/2020GC009251

Shaar, R., Tauxe, L., Goguitchaichvili, A., Devidze, M., & Licheli, V. (2017). Further evidence of the Levantine Iron Age geomagnetic anomaly from Georgian pottery. *Geophysical Research Letters*, *44*(5), 2229–2236.

Suttie, N., & Nilsson, A. (2019). Archaeomagnetic data: The propagation of an error. *Physics of the Earth and Planetary Interiors*, *289*, 73–74.

Talarn, À., Pavón-Carrasco, F. J., Torta, J. M., & Catalán, M. (2017). Evaluation of using R-SCHA to simultaneously model main field and secular variation multilevel geomagnetic data for the North Atlantic. *Physics of the Earth and Planetary Interiors*, *263*, 55–68.

Tema, E., Hedley, I., Pavón-Carrasco, F. J., Ferrara, E., Gaber, P., Pilides, D., et al. (2021). The directional occurrence of the Levantine geomagnetic field anomaly: New data from Cyprus and abrupt directional changes. *Earth and Planetary Science Letters*, *557*, 116731.

Thébault, E. (2008). A proposal for regional modelling at the Earth's surface, R-SCHA2D. *Geophysical Journal International*, *174*(1), 118–134.

Thébault, E., Finlay, C. C., Beggan, C. D., Alken, P., Aubert, J., Barrois, O., et al. (2015). International geomagnetic reference field: The 12th generation. Earth. *Planets and Space*, *67*(1), 1–19.

Thébault, E., & Gaya-Piqué, L. (2008). Applied comparisons between SCHA and R-SCHA regional modeling techniques. *Geochemistry, Geophysics, Geosystems*, *9*(7). https://doi.org/10.1029/2008GC001953

Thébault, E., Mandea, M., & Schott, J. J. (2006). Modeling the lithospheric magnetic field over France by means of revised spherical cap harmonic analysis (R-SCHA). *Journal of Geophysical Research*, *111*. https://doi.org/10.1029/2005JB004110

Thellier, E., & Thellier, O. (1959). Sur l'intensité du champ magnétique terrestre dans le passé historique et géologique. *Annales de Geophysique*, *15*, 285–376.